Journal of Thermal Analysis and Calorimetry, Vol. 95 (2009) 1, 69–74

THERMAL STABILITY AND SURFACE STRUCTURE OF Mo/CeO_2 AND Ce-DOPED Mo/Al_2O_3 CATALYSTS

H. Nasser, Á. Rédey, Tatiana Yuzhakova and J. Kovács*

Institutional Department of Environmental Engineering and Chemical Technology, University of Pannonia, Veszprém P.O. 158, 8201 Hungary

In order to explore the influence of CeO_2 on the structure and surface characteristics of molybdena, an investigation was undertaken by using N_2 adsorption (BET method), thermal analysis and in-situ diffuse reflectance infrared (DRIFT) techniques. In this work, the Mo/CeO_2 and $Ce–Mo/Al_2O_3$ samples were prepared by impregnation and co-precipitation methods with high Mo loadings. Combining the results one may notice that the presence of ceria led to the increase of polymerized surface Mo species so as to forming Mo–O–Ce linkages besides the formation of coupled O=Mo=O bonds indicative of polymeric MoO_3.

From thermal analysis, it can be inferred that Mo/Al_2O_3 is the thermally most stable material in the temperature range used in the experiment (up to 900°C), whereas $Ce–Mo/Al_2O_3$ and Mo/CeO_2 samples undergo morphological modifications above 700°C resulting in lattice defects, which motivate the mobility of Mo and Ce ions and thus enhance the possibility of interaction between them. Additionally, their activity towards CO adsorption needs reduced ceria and molybdena containing coordinatively unsaturated sites (CUS), oxygen vacancies and hydroxyl groups to form various carbonate species.

Keywords: *CO adsorption, DRIFT, molybdena-ceria, TG-DTA*

Introduction

Presently, there is a continuous interest in Mo-containing catalysts due to their potential role in many industrial applications such as hydrodesulphurization (HDS), oxidative dehydrogenation (ODH), isomerization and partial oxidation of alkanes. On the basis of previous studies, it is generally known that the surface of molybdena remains mainly containing monomeric Mo species. Moreover, polymeric molybdate species and free MoO_3 can be formed at high Mo contents taking into account the calcination temperature and time as well as the solution pH, the isoelectric point and surface area of the solid support [1, 2].

Semiconductive oxides are widely used in heterogeneous catalysis either as supports or active phases. In the case of *n*-type semiconductors (e.g. CeO_2, SnO_2) when heated in reducing atmosphere (e.g. H_2, CO) become non-stoichiometric by losing oxygen, which generates cations with unsaturated coordination, thus increases the free electron concentration [3, 4].

Their mid-infrared examination offers special difficulties mainly due to their transition types, which involve the absorbance due to free carriers and electron- or hole-donors, whose concentration depends on the semiconduction type, the surrounding atmosphere and the temperature. These difficulties are seriously enhanced when the sample under study is a metal supported on an *n*-type semiconducting support, the reduction of the support is then greatly favoured by the metal, e.g. through activation in vacuum and spill over of hydrogen or CO. It follows that the absorbance may decrease to zero, especially when the reducing gas is adsorbed at temperature higher than the ambient [4–10].

CeO_2 in addition to its role either as oxygen storage and release or thermal stabilizer. It has been used either as a promoter or a support for metal catalysts in many applications since ceria has a beneficial effect for CO oxidation and NO_x reduction under both stoichiometry and excess oxygen besides for CO/NO reaction, CO and CO_2 hydrogenation, this acquired a tremendous attraction particularly in connection with world-wide endeavors to curb the detrimental impacts of automotive emissions on the atmosphere [6–11].

Many researchers clearly assigned the promotional effect of the catalysts to the role of ceria in creating Ce^{3+}/Ce^{4+} redox couple [10–15]. However, an attention has been given to transition metals and their oxides as catalysts supported on CeO_2 or doped with CeO_2, since the ability of ceria to donate oxygen to supported metals is also a key feature in other catalytic reactions like catalytic combustion and water gas shift reaction [12, 13].

Despite numerous studies devoted to molybdena and ceria a lot of debates concerning the role played by ceria oxide necessitate further studies for better understanding the nature, structure and the

* Author for correspondence: heider@almos.vein.hu

1388–6150/$20.00

Akadémiai Kiadó, Budapest, Hungary
Springer, Dordrecht, The Netherlands

physico-chemical properties of these catalysts, since the nature of the interactions between metal oxides and supports are often attributed to the complexity of these systems and differences in the experimental conditions adopted.

Experimental

Catalyst preparation

The γ-Al_2O_3 (Ketjen CK300) and CeO_2 formed by the thermal decomposition of $Ce(NO_3)_3 \cdot 6H_2O$ (Lobo Feinchemie) in air at 600°C for 6 h were used as supports for catalyst preparation. The Mo/Al_2O_3 and Mo/CeO_2 catalysts were prepared by the impregnation of the supports (γ-Al_2O_3, CeO_2) with an aqueous ammonium heptamolybdate $(NH_4)_6\ Mo_7O_{24} \cdot 4H_2O$ (Merck) solution at pH=2. The concentration of heptamolybdate was that required not only to obtain surface concentrations close to the theoretical monolayer coverage but also go beyond a compact single lamella of molybdenum oxide structure. The contact time for a given concentration with the solid (γ-Al_2O_3, CeO_2) was extended for 72 h and the temperature of the rotary shaker was maintained at 25°C. In the second method, a co-precipitation of CeO_2 and Mo/Al_2O_3 by adding 10 *v*/*v*% HNO_3 was achieved to prepare 5 mass% Ce–20 mass% Mo/Al_2O_3 sample. All samples were dried in air at 150°C for 6 h followed by calcination in air at 600°C for 12 h.

Catalyst characterization

a) Inductive coupled plasma-atomic absorption spectroscopy (ICP-AAS) was performed in order to verify the amounts of Mo loading using Unicam apparatus. Therefore, the molybdenum loading was 20 mass% in Mo/Al_2O_3 and 12 mass% in Mo/CeO_2 samples.

b) Total surface area, S_{BET}, was calculated using the multipoint BET analysis method. The assessment of mesoporosity was estimated from the adsorption branches via BJH method. The nitrogen adsorption/desorption isotherms were measured at –196°C using a conventional volumetric apparatus.

c) TG and DTA analyses were conducted for 50 mg of uncalcined samples using automatically recorded Labsys-TG (France) units. The rate of heating was 10°C min^{-1} under a flow of dry air (Messer, Hungary) from room temperature up to 900°C.

d) Diffuse reflectance Fourier transform infrared (DRIFT) spectroscopic studies were performed by Bruker Tensor 27 spectrometer with an air cooled DTGS detector. In all cases, in situ DRIFT spectra were recorded using Thermo-Nicolet DRIFT cell by co-addition of 126 scans at 4 cm^{-1} resolution. The cell equipped with Thermo chamber specially designed for high temperature/vacuum studies (up to 900°C) was fitted with KBr disks for low temperature and CaF_2 disks for high temperature measurements. The operating temperature with deviation of ±3°C was controlled by using Thermo-Nicolet proportional temperature controller connected to the cell. In situ DRIFT spectra expressed as absorbance unit *vs*. frequency were collected after taking the background spectrum for each experiment and can be evaluated accordingly. Spectral manipulations such as baseline correction, smoothing, normalization, band component analysis and deconvolution were performed using 'OPUS' and 'GRAMS' software packages. Hence, the cell was attached to a glass gas handling/ultrahigh vacuum system and can be evacuated up to 10^{-5} Torr. Thus, with the aid of this system the following gases were used for treatments and reactions:

- Reduction in hydrogen (Messer, purity of 99.995%)
- CO (Messer, purity of 99.99%)
- O_2 and N_2 (Messer, purity of 99.6%)

Results and discussion

Surface texturing

The Mo surface density is expressed as the number of Mo atoms per nanometer square of surface area (Mo atoms nm^{-2}). It was obtained by the equation [2]:

$$\text{Mo surface density} = \frac{MoO_3\,\text{mass}\% \cdot 6.02 \cdot 10^{23}}{\text{surface area} \cdot 144 \cdot 10^{18}}$$

where the unit of the surface area is $m^2\ g^{-1}$ and 144 is the molar mass of MoO_3. The values of surface areas, total pore volume, V_p ($cm^3\ g^{-1}$) and the average mesopore diameter for the calcined materials were estimated and cited in Table 1, whereas Fig. 1 shows the mesopore volume distribution in $dV/d\log(D)$ *vs.* pore diameter plot of these samples. The Mo/Al_2O_3 catalyst has an average mesopore diameter around 6.2 nm and a continuous distribution of larger pores that extends well into the macroporous region. As this sample contains high Mo amount, its texture may be related to Al_2O_3 because the pore size distribution curve obtained for Al_2O_3 (not shown) is very similar. Accordingly, it may be inferred that the large pores present in the Mo/Al_2O_3 sample may be related to the interstices resulting from the packing of the Al_2O_3 particles which behave as pores in the N_2 adsorption measurements.

More specifically, upon addition of cerium the average mesopore size increased in $Ce–Mo/Al_2O_3$ sample. This increase is responsible for the significant reduction of the specific surface area of this sample (Table 1). However, increasing the wide pore diameter of the for-

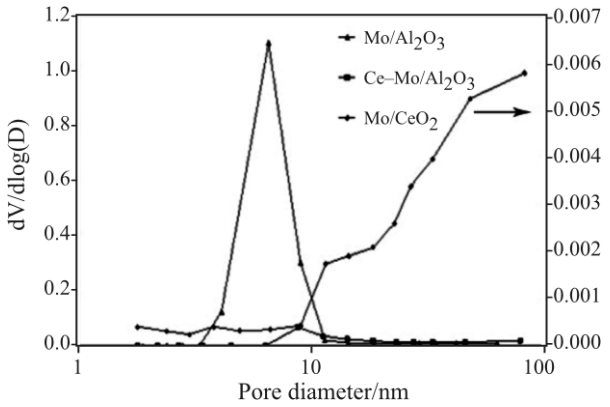

Fig. 1 Logarithmic mesopore volume distribution *vs.* pore diameter

mer sample is indicative to the role played by cerium–molybdate and CeO_2 and to their partial deposition inside the micropore creating their own pore system and thus enhancing the pore diameter. Additionally, these species might be deposited on internal surfaces blocking some pores in Ce–Mo/Al_2O_3 and thus, reducing the surface area comparatively. Nevertheless, some Mo nanoparticles presumably entrapped in the micropores of ceria oxide that can also cause expansion in unit cell and pore diameter. On the other hand, the pore diameter size remained almost unchanged for Mo/CeO_2 sample in comparison with CeO_2. This may propose that the diffusion of MoO_3 did not proceed into the bulk CeO_2 during the preparation. However, inspecting of the data compiled in Table 1 reveals the mesoporosity nature of these materials and decreasing the total pore volume of all samples comparatively may indicate that their pores are narrow as well as they are deep [8, 12].

Thermal analysis

The thermogravimetric (mass loss, TG), derivative thermogravimetric (rate of mass loss, DTG) and differential thermal analysis (DTA) curves of uncalcined samples, over the range from room temperature up to 900°C in the flow of dry air, are shown in Figs 2–4. The recorded TG and DTA curves of Mo/Al_2O_3 (Fig. 2) exhibit a large mass loss (37.8%) up to 270°C that was resolved into endothermic peak of maxima at 83°C in the DTA curve. This is corresponding, respectively, to the loss of structural and intercalated water and to the decomposition of $(NH_4)_6Mo_7O_{24}\cdot 4H_2O$. The DTA curve of this sample displays a big exothermic peak of a maximum at around 300°C that could be due to the process of the formation of new phases probably to the crystallization of MoO_3 species.

The TG and DTA curves recorded for Ce–Mo/Al_2O_3 (Fig. 3) indicate that the mass loss value (20.5%) under 300°C is less than that of Mo/Al_2O_3. This mass loss is due to the removal of water and to the decomposition of $Ce(NO_3)_3$ and $(NH_4)_6Mo_7O_{24}\cdot 4H_2O$ producing the corresponding oxides according to:

$$(NH_4)_6Mo_7O_{24}\cdot 4H_2O+Ce(NO_3)_3+2O_2\rightarrow 7MoO_3+CeO_2+3NO_2+6NH_3+12H_2O$$

In the meanwhile, the position of the endothermic peak shifts to a higher value with maxima at 101°C, whereas the big exothermic peak remained with the maximum at around 300°C comparatively. Of particular interest, the TG and DTA curves of Ce–Mo/Al_2O_3 display a mass loss (23%) extended between 700 and 900°C with an endothermic peak of maxima at 758°C.

The thermal decomposition course presented for Mo/CeO_2 is shown to be of multistep and represented by four endothermic peaks of maxima at 61, 98, 173 and 737°C in the DTA curve (Fig. 4) besides an exothermic peak of a maximum at 308°C. As can be seen, this material contributes a total mass loss around 34.7%. However, the endothermic peaks present above 700°C in DTA curves of Ce–Mo/Al_2O_3 (758°C) and Mo/CeO_2 (737°C) indicate that the materials undergo morphological modifications and lattice defects. Thus, the crystalline structure is progressively modified comparatively favouring the possible mutual diffusion of the Mo and Ce ions. The last mass loss in these materials may characterize the sublimation of some molybdena produced [6, 16–19].

On the other hand, it is worth mentioning that the decomposition temperature of either Mo or Ce precursor salts in the synthesized materials are not similar revealing that the interactions between them are varied according to altering the preparation methods

Table 1 Textural characteristics derived from BET method for the materials calcined at 600°C

Catalyst	Average pore diameter/nm	Total mesopore volume/$cm^3\ g^{-1}$	BET surface area/ $m^2\ g^{-1}$	Mo density/ atom nm^{-2}
γ-Al_2O_3	6.37	0.51	200	–
20 mass% Mo/Al_2O_3	6.2	0.225	117.6	7
5 mass% Ce–20 mass% Mo/Al_2O_3	6.9	0.072	29.6	28
CeO_2	12.8	0.016	80	–
12 mass% Mo/CeO_2	12.5	0.0053	16.2	31

and their content, which indeed affect the mobility of Mo and Ce species that in turn affects the interaction mode of CeO_2–MoO_3 compounds. The latter affects by its turn the thermal stability of the produced compounds. Accordingly, although the type of active sites is more or less similar in all samples, different reaction pathways may result in different activities.

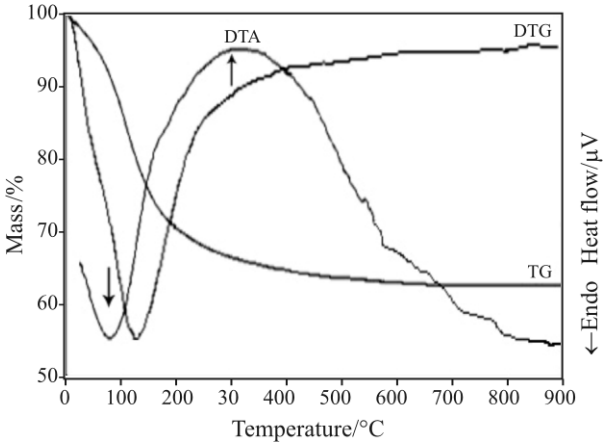

Fig. 2 TG, DTG and DTA curves of Mo/Al_2O_3

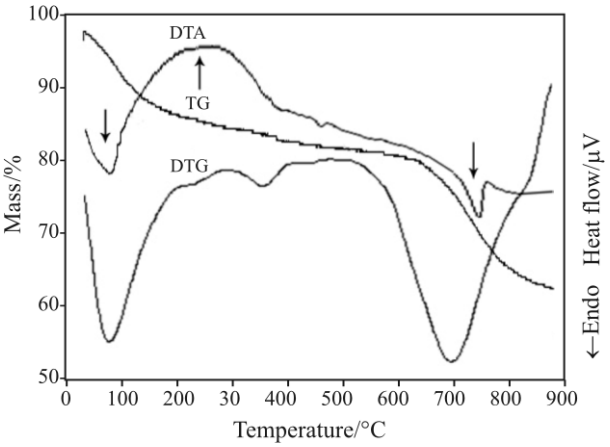

Fig. 3 TG, DTG and DTA curves of $Ce–Mo/Al_2O_3$

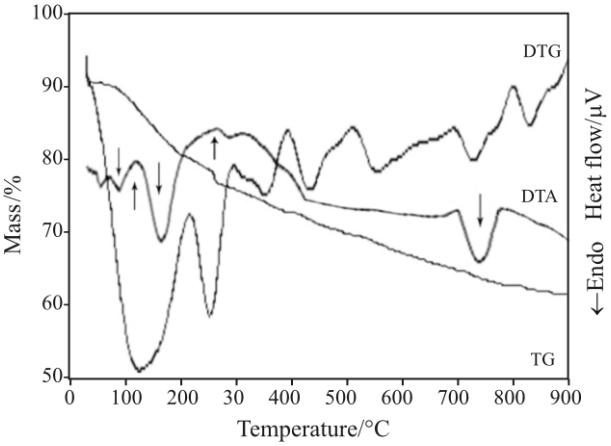

Fig. 4 TG, DTG and DTA curves of Mo/CeO_2

In situ DRIFT spectroscopy measurements

The DRIFT spectra of the samples calcined at 600°C after evacuation at 10^{-5} Torr and room temperature are depicted in Fig. 5. The spectrum of Mo/Al_2O_3 shows bands at 415 and 490 cm^{-1} corresponding to bridging stretching modes of $\nu_{s(Mo\text{-}O\text{-}Al)}$ and $\nu_{as(Mo\text{-}O\text{-}Al)}$ indicating the strong association of Mo species (MoO_4^{2-}) with Al_2O_3 support. On the other hand, the band at 995 cm^{-1} corresponding to $\nu_{as(Mo=O)}$ terminal stretching in bulk MoO_3 indicates strong features for microcrystalline MoO_3 species [6, 7]. However, the absence of Mo=O stretches corresponding to tetrahedral MoO_4^{2-} species bonded to alumina surface, which undoubtedly appear at 950–955 cm^{-1} confirms the evidence for the appearance of polymeric MoO_4^{2-} that is further emphasized by the band appearing at 749 cm^{-1} assigned to $\nu_{s(Mo–O–Mo)}$ which shifts to higher frequency (757 cm^{-1}) in $Ce–Mo/Al_2O_3$ spectrum [2, 4–8].

The spectra of Mo/CeO_2 and $Ce–Mo/Al_2O_3$ exhibit characteristic IR bands and 480 cm^{-1} due to asymmetric streching modes of ν_{as}(Ce–O) terminal bonds, while the bands at 690 and 740 cm^{-1} are assigned to ν_s(Ce–O–Ce) and ν_{as}(Ce–O–Ce) bridging bonds. However, the fact that the addition of ceria contributes to the formation of new phases so as to forming Mo–O–Ce linkages that were represented by the bands at 630 cm^{-1} $\nu_{s(Mo–O–Ce)}$ and 875 cm^{-1} $\nu_{as(Mo–O–Ce)}$, while the bands separated by 40 cm^{-1} with different relative intensities at 995 and 1035 cm^{-1} are associated with the formation of coupled $\nu_{s(O=Mo=O)}$ bonds indicative of polymeric MoO_3.

Accordingly, ceria can attribute to the increase of polymerized surface Mo species. Nevertheless, the expected competition between Ce and Mo with alumina hydroxyl groups may suppress stronger interactions between them (decreased OH intensity in the $Ce–Mo/Al_2O_3$). Details of OH yield on alumina and ceria have been given elsewhere [2, 5–9].

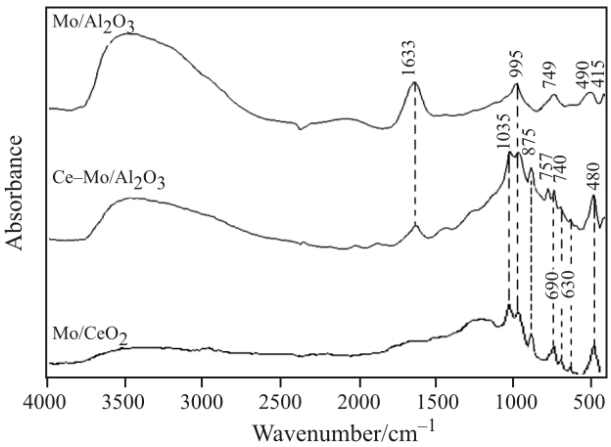

Fig. 5 In situ DRIFT spectra of the catalysts calcined at 600°C

CO adsorption on Mo/CeO_2, Ce–Mo/Al_2O_3 and CeO_2 catalysts reduced at 800°C

The experimental procedure was performed for all samples as follows:

- The sample was mounted in the cell fitted with CaF_2 disks (IR transparency>1000 cm^{-1}). After evacuation at about 10^{-5} Torr for 30 min the sample was reduced at 800°C in hydrogen flow (60 cm^3 min^{-1}, 1 bar, 10°C min^{-1} of heating rate) for 1 h.
- The system was cooled back to room temperature, flushed with N_2, then evacuated at room temperature and 10^{-5} Torr for 30 min.
- Hence, the CO adsorption was performed at 30 Torr and in temperature range 20-100°C for one h. All the DRIFT spectra (MIR) of adsorbed CO are preserved following evacuation of the cell at room temperature and 10^{-5} Torr for 30 min.

On the other hand, since no appreciable CO adsorption bands appeared (except Ce^{4+}–CO, Ce^{3+}–CO) below 100°C only the spectra of CO adsorption at 100°C are subtracted and deconvoluted (Fig. 6). On the basis of the results that can be found extensively in the literature regarding the reduction of Mo and Ce [1–5] CO adsorption was performed on the catalysts reduced at 800°C.

In situ DRIFT measurements of CO adsorption exhibit reactivity pattern initiating from adsorbed CO and various types of carbonate on catalysts reduced at 800°C. The spectrum of Ce–Mo/Al_2O_3 exhibits an indicative band at 2198 cm^{-1} of coordinatively unsaturated (CUS) octahedral Al^{3+} sites, whereas a band at 2170 cm^{-1} is attributed to CO linearly bonded to Ce^{4+} cations that is observed in all Ce-containing catalysts. On the basis of spectral investigations of various carbonate compounds that can be found elsewhere [10, 13], one can suppose that the surface of Ce–Mo/Al_2O_3 is covered with various types of carbonate: monodentate (ν_s1420, ν_{as}1540 cm^{-1}), bidentate (ν_{as}1320, ν_s1680 cm^{-1}) and bicarbonate (ν_s1460, ν_{as}1630 and 1220 cm^{-1} γ_{OH}). The DRIFT spectra recorded on reduced CeO_2 and Mo/CeO_2 following CO adsorption show a band at 2150 cm^{-1} assigned to linearly bonded CO to Ce^{3+} together with the band assigned to Ce^{4+}-CO besides the band at 2025 cm^{-1} due to CO adsorbed to metallic Mo^0. One can notice that the reduced surface of CeO_2 and Mo/CeO_2 after CO chemisorption exposes clearly monodentate carbonate (ν_s1430, ν_{as}1570 cm^{-1}), bidentate (ν_{as}1340, ν_s1680 and ν_{as}1320, ν_s1690 cm^{-1}), bicarbonate (1220, 1230 cm^{-1} γ_{OH}, ν_s1460, ν_s1490 and ν_{as}1630 cm^{-1}), and bridged carbonate (ν_{as}1285 and ν_s1750 cm^{-1}). Of particular interest, the CO adsorption on Mo/CeO_2 shifts the corresponding peak positions to higher wavenumbers implying the increase in CO surface coverage and different distribution of electrons

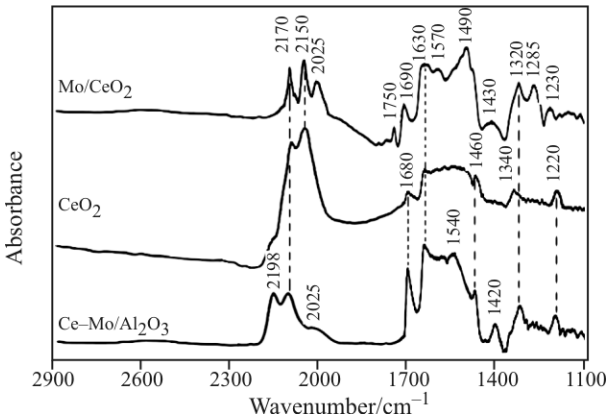

Fig. 6 In situ DRIFT spectra of CO adsorbed at 100°C and 30 Torr

comparatively. The reduction of the catalysts to produce lower oxidation states of Mo and more Ce^{3+} species activated the surface to be eligible for CO adsorption as metal–CO as well as carbonate species being stable under vacuum at room temperature. Thus, CO adsorption involves oxygen in the catalysts such oxygen could be present in Mo=O, Mo–O–Mo, Ce–O–Mo and Ce–O–Ce associates [14, 20].

However, the absence of Ce^{3+}–CO band in Ce–Mo/Al_2O_3 spectrum indicates that Ce ions are preferentially located in the internal surface of Al_2O_3 particles and mostly in compensating positions substituting Mo ions in Ce–Mo/Al_2O_3 whereas for Mo/CeO_2 the majority of Ce ions are present on the external surface as cerium–molybdenate and CeO_2 moieties. Therefore, it can be anticipated that the formation of various carbonates needs reduced ceria and molybdena containing oxygen vacancies and hydroxyl groups. Thus, CO being provided as weakly adsorbed metal-carbonyls migrating towards the oxides through interfacial sites to form carbonates via (LH) mechanism. Furthermore, the interaction between Mo and supports has an effect on the adsorption properties of CO, which may indicate the different electronic effects in the catalysts. Within this context, intimate coupling of Mo and Ce ions of different oxidation states has great facilities for electron exchange interactions enhancing the CO adsorption. On the other hand, the geometric effects also play an important role for the Mo-support interactions, the variance of the reducibility may be caused by the different locations of Mo on the supports or the different orientations of Mo combination to the supports. The special Ce–Mo–Al interaction may be originated from both the electronic effect that affects the CO adsorption and the geometric effect that may contribute to the reducibility variance of MoO_3. Furthermore, different methods for sample preparation and pre-treatment will result in surfaces with different orientations, different oxidation states (e.g. unreduced and

reduced), and varying degrees of surface contamination [15]. Defects such as step edges, vacancies and partial surface reconstructions allow for the formation of surface carbonates on the surfaces.

Conclusions

One may suggest that the introduction of cerium promotes aggregation of the Mo particles (mainly as a support) probably due to charge effects and/or the strong basic property possessed by CeO_2 as further emphasized by means of DRIFT (Mo–O–Ce linkages and coupled O=Mo=O bonds). However, Mo/Al_2O_3 material showed the highest thermal stability while the others undergo structural modifications above 700°C. This may be due to the high oxygen storage and release of ceria resulting in lattice defects and thus enhancing the mobility of Mo and Ce ions. Moreover, the fact that the three samples showed varying net mass loss implying that they have not comparable molecular formulae according to altering the preparation method and their content. On the other hand, the hydrogen reduction of the catalysts at 800°C improves the surface reactivity leading to the presence of metallic Mo species and oxygen vacancies and thus enhancing CO adsorption. It is reasonable to suggest that the CO adsorption may proceed through a surface reaction between the weakly adsorbed CO to metal species and the surface lattice oxygen via the Langmuir–Hinshelwood (LH) mechanism to form large amounts of carbonate species implying the existence of reactive lattice oxygen that may be due to the weakening of the covalence of the metal–oxygen lattice bonds and/or the enhancement of the mobility of lattice oxygen sites induced by H_2 reduction. Additionally, the electron-mobile environment necessitated by redox reactions between Mo and Ce ions is established that has a great share in enhancing the CO adsorption.

References

1 Á. Rédey and W. K. Hall, J. Catal., 108 (1987) 185.
2 L. Wang and W. K. Hall, J. Catal., 77 (1982) 232.
3 G. Busca, Catal. Today, 41 (1998) 191.
4 J. Ryczkowski, Catal. Today, 68 (2001) 263.
5 G. A. Lucia, F. M. Goncalves and P. R. S. Medeiros, Appl. Catal. A, 208 (2001) 265.
6 M. M. Mohamed, Appl. Catal. A, 267 (2004) 135.
7 M. M. Mohamed and S. M. A. Katib, Appl. Catal. A, 287 (2005) 236.
8 K. M. S. Khalil, J. Colloid Interface Sci., 307 (2007) 172.
9 R. Craciun, W. Daniell and H. Knözinger, Appl. Catal. A, 230 (2002) 153.
10 J. Kristóf, H. Nasser, R. L. Frost, A. De Battisti and Á. Rédey, Appl. Surf. Sci., 242 (2005) 13.
11 H. Zhu, Z. Qin, W. Shan, W. Shen and J. Wang, J. Catal., 233 (2005) 41.
12 A. Zecchina, C. Lamberti and S. Bordiga, Catal. Today, 41 (1998) 169.
13 S. Yokota, K. Okumura and M. Niwa, Catal. Lett., 84 (2002) 131.
14 S. Chempath and A. T. Bell, J. Catal., 247 (2007) 119.
15 Z. Yang, T. K. Woo and K. Hermansson, Chem. Phys. Lett., 396 (2004) 384.
16 E. Horváth, J. Kristóf, N. Heider, R. L. Frost and V. Vágvölgyi, J. Therm. Anal. Cal., 78 (2004) 687.
17 Z. Sarbak and W. K. Józwiak, J. Therm. Anal. Cal., 87 (2007) 229.
18 R. Lyszczek, J. Therm. Anal. Cal., 90 (2007) 533.
19 M. Blachnio, P. Staszczuk, G. Grodzicka, L. Lin and Y. X. Zhu, J. Therm. Anal. Cal., 88 (2007) 601.
20 H. Nasser, Á. Rédey, T. Yuzhakova, Zs. N. Tóth and T. Ollár, React. Kinet. Catal. Lett., 92 (2007) 329.

Received: February 5, 2008
Accepted: April 26, 2008
OnlineFirst: August 15, 2008

DOI: 10.1007/s10973-008-9050-y